DMD Fast Forward. Published on March 26, 2022 as DOI: 10.1124/dmd.122.000831
This article has not been copyedited and formatted. The final version may differ from this version.

DMD-AR-2022-000831

Predicting impact of food and feeding time on oral absorption of drugs with a novel rat continuous intestinal absorption model

Casey Radice, Ken Korzekwa, and Swati Nagar

Department of Pharmaceutical Sciences, Temple University School of Pharmacy, Philadelphia PA 19140, USA

DMD-AR-2022-000831

Running Title

Predicting food impact on oral absorption in rats

Corresponding Author:

Swati Nagar, PhD

Department of Pharmaceutical Sciences, Temple University School of Pharmacy

3307 N Broad Street, Philadelphia PA 19140, USA

Phone: 215-707-9110

Email: swati.nagar@temple.edu

Number of text pages: 46

Number of tables: 3

Number of figures: 7

Number of references: 45

Number of words in

Abstract: 250

Significance statement: 73

Introduction: 722

Discussion: 1393

List of non-standard abbreviations

ACN - acetonitrile

AICc – corrected Akaike information criterion

AML – amlodipine

AUC – area under the curve

BCS – biopharmaceutics classification system

C-t – concentration-time profile

CE – collision energy

CXP – collision cell exit potential

DIG – digoxin

DP – dispersion potential

EOC – exposure overlap coefficient

FT – feeding time

HPLC – high performance liquid chromatography

IV – intravenous

LC-MS/MS – liquid chromatography and tandem mass spectrometry

LLOQ – lower limit of quantitation

Oatp – organic anion transporter protein

ODE – ordinary differential equationssu

PBPK – physiologically based pharmacokinetic models

PDE – partial differential equations

Pgp – p-glycoprotein

PK – pharmacokinetics

PO - peroral

Abstract

Intricacies in intestinal physiology, drug properties, and food effects should be incorporated into models to predict complex oral drug absorption. A previously published human continuous intestinal absorption model based on the convection-diffusion equation was modified specifically for the male Sprague-Dawley rat in this report. Species-specific physiological conditions along intestinal length 'x' - experimental velocity and pH under fasted and fed conditions, were measured and incorporated into the intestinal absorption model. Concentration- time (C-t) profiles were measured upon a single IV and PO dose for three drugs, amlodipine (AML), digoxin (DIG), and glyburide (GLY). Absorption profiles were predicted and compared with experimentally collected data under three feeding conditions: 12-hr fasted rats were provided food at two specific times after oral drug dose (1 hr and 2 hr for AML and GLY, 0.5 hr and 1 hr for DIG), or were provided food for the entire study. IV versus PO C-t profiles suggested absorption even at later times, and informed design of appropriate mathematical input functions based on experimental feeding times. With this model, AML, DIG and GLY oral C-t profiles for all feeding groups were generally well predicted, with exposure overlap coefficients (EOC) in the range of 0.80 – 0.97. Efflux transport for DIG and uptake and efflux transport for GLY were included, modeling uptake transporter inhibition in the presence of food. Results indicate that the continuous intestinal rat model incorporates complex physiological processes and feeding times relative to drug dose, into a simple framework to provide accurate prediction of oral absorption.

Significance Statement

A novel rat continuous intestinal model predicts drug absorption with respect to time and intestinal length. Feeding time relative to dose was modeled as a key effect. Experimental fasted/fed intestinal pH and velocity, efflux and uptake transporter expression along intestinal length, and uptake transporter inhibition in the presence of food, were modeled. The model uses the pharmacokinetic profiles of three model drugs and provides a novel framework to study food effects on absorption.

Introduction

Most drugs are administered orally due to cost-efficacy, non-invasiveness, and increased patient compliance (Alqahtani et al., 2021). However, orally administered drugs are subject to complex biological processes, and their absorption additionally depends on the physicochemical properties of the dosed drug. Biological parameters contributing to complex intestinal absorption kinetics include gastrointestinal transit, presence and type of food, pH, and transporter expression. Drug properties such as lipophilicity, pKa, along with permeability, solubility, and formulation are also impactful.

One of the most notable contributors to the difficulty of absorption predictions is the effect of food (Welling, 1977; Higashi et al., 2013; Owens et al., 2021). Food has been known to affect gastric emptying, small intestinal transit, pH, blood flow, transporter expression, and can even act as a mechanical barrier or binder (Ward and Coates, 1987; Klein, 2010; Dou et al., 2018). Food effects may explain the inter-lab variability seen in PK profiles for the same drug at the same dose (Li et al., 2012; Jiang et al., 2015). Preclinical pharmacokinetic (PK) studies are typically performed in fasted rats to reduce the inter-animal variability in C-t profiles (Melander, 1978; Singh et al., 2011; Small et al., 2015). Animals are usually fasted overnight between 12 and 18 hours, which is often noted (Vermeulen et al., 1997). However, most reports fail to specify when animals were fed after drug administration. Further, while rats show similar intestinal permeability and drug absorption as humans (Cao et al., 2006), the usefulness of rat studies is diminished by differences in species-specific physiological parameters such as transporters. Further, rat anatomy and physiology are markedly different from human especially regarding the rat versus human stomach, and with the presence (human) versus absence (rats) of a gall bladder (DeSesso and Jacobson, 2001; Vdoviakova et al., 2016).

Prediction of PK parameters utilizes a range of modeling methods including classic compartmental models and physiologically-based pharmacokinetic (PBPK) models, where compartments represent specific organs or tissues which are connected by blood flows (Lin and Wong, 2017). Hybrid models include the target organ explicitly, while the remainder of the body is modeled as mathematical compartments. The most widely used absorption model in humans are the Advanced Compartmental Absorption and Transit (ACAT) and Advanced Dissolution Absorption and Metabolism (ADAM) models, which model the intestine as a series of compartments (Huang et al., 2009). Physiological factors (pH, gastric emptying, intestinal transit, and transporter expression levels) and physicochemical factors (pKa, particle size, and solubility) are integrated into the model to predict absorption. This model uses ordinary differential equations to predict drug movement in the body. Another approach is to consider the intestine to be a continuous compartment. Absorption is modeled as a change in drug concentration along distance (x) and over time (t) (Nagar et al., 2017). This continuous absorption model was developed based on the convection-diffusion equation (Ni et al., 1980), and is based on partial differential equations (PDEs), which were revisited due to the advancements in computational power and speed. Physiological parameters are described as functions of distance x and can vary along the length of the intestine.

The goal of the current work was to develop a mathematical framework for predicting the impact of food and feeding time on oral drug absorption. Our previously published human continuous intestinal model was first modified to create a rat model. The collection of rich physiological and PK data to develop and refine a rodent model is feasible and provides useful proof-of-concept data, whereas similar data collection may be cost-prohibitive or not possible in humans. Rat gastro-intestinal anatomy and physiology data were collected and used to build the rat model.

Next, three model drugs – amlodipine (AML), digoxin (DIG), and glyburide (GLY) – were dosed IV as well as PO, and concentration-time datasets were collected. The drugs were selected based on differences in their solubility, permeability, and rat transporter profiles. AML is a BCS class 1 drug and is not a reported transporter substrate in rats. DIG is BCS class 4 and a Pgp substrate. GLY is BCS class 2 and a Pgp and Oatp substrate (El-Kattan and Varma, 2011; Estudante et al., 2013; Suzuki et al., 2014). All datasets were collected at various feeding times post-dose. A rat continuous absorption model was developed, and the observed impact of food and feeding time relative to drug dosing on drug absorption was modeled with the absorption model.

Materials and Methods

Chemicals and reagents

Amlodipine was purchased from Alfa Asear (Haverhill, MA). Glyburide was from Frontier Scientific (Logan, UT). Digoxin was obtained from Tocris (Ellisville, MO). Glyburide-d3 and digoxin-d3 were purchased from Cayman Chemical (Ann Arbor, MI). Amlodipine-d4 was obtained from Toronto Research Chemicals (North York, Canada). Sprague Dawley (SD) rat plasma was purchased from Equitech Biotech Inc (Kerrville, TX). Polyethylene glycol 400 (PEG-400) and methylcellulose (viscosity 400cP) were from Sigma-Aldrich (St. Louis, MO). 1-methyl-2-pyrrolidinone (NMP) is from J.T baker (Allentown, PA).

Animals

Male Sprague-Dawley single jugular cannulated rats weighing 239 – 250g were ordered from Charles River (Wilmington, MA). All rats were singly housed under a reverse 12-hour light/dark cycle. Rats were acclimated for at least four days in the Temple University Health Sciences Campus animal housing facility and 30 minutes in the procedure room prior to the start of the study. Food (standard rodent chow) and water were available ad libitum for fed groups. Food was removed from the cages of fasted groups 12 hours before the beginning of the study. All animal studies were performed with strict adherence to protocols approved by the Temple University IACUC. The total number of animals used was minimized by using the same animal for intestinal measurements after the completion of pharmacokinetic studies.

Rat intestinal measurements

<u>Intestinal dimensions and pH determination</u>

Rats were sacrificed, and their intestines were clamped at the pyloric sphincter and most distal portion of the colon to prevent bodily fluids from entering and influencing pH. The intestines were removed and divided into ten unequal segments. The small intestine was divided into seven segments. The first 10 cm, starting from the pylorus, was labeled the duodenum. The last 3 cm, ending at the cecum, was considered the ileum. The middle portion was divided into five equal parts, with jejunum 1 (J1) starting at the end of the duodenum and jejunum (J5) ending at the start of the ileum. The colon was divided into two equal sections: proximal and distal. The cecum was separately isolated. After pH measurements described below, the intestines were cut along the length to lay flat, taking care not to overstretch the organs. The lengths of the small intestine (n=43) and colon (n=14) were measured with a tape measurer and recorded. Each segment's width (n=5) was also collected by measuring the distance from one side of the cut to another, perpendicular to the length.

For pH measurement, the luminal contents were removed from each segment by lightly squeezing each segment with a pair of tweezers. A single, similarly-sized fecal pellet in the distal colon was mixed with 0.5 ml of water and vortexed to obtain a homogenous mixture for each rat. No water was added to any other segment. After initial pH measurements, an extra 0.5 mL of water was added to assess the influence of the water on the pH for one rat in each group. The pH of the luminal contents was measured using a pre-calibrated pH meter between one and three times, remixing between each reading. The order of the segments measured was alternated between animals to minimize post-mortem pH drift.

The pH of the food pellets was measured on two separate days to determine the influence of pellet pH on luminal pH. Three standard size rat pellets (~12 g) were placed in a tube containing 10 mL of water. The pellets were vortexed until entirely disintegrated and no solid pieces could

be seen. The pH of the pellet mixture was measured three times, shaking the mixture between measurements.

Gastrointestinal motility

Rats (n=36) were divided into one of two condition groups: fasted or fed. Fed (n=17) and 12-hour fasted (n=19) male Sprague-Dawley rats were administered 0.5 mL of a 5% activated charcoal in 1.5% methylcellulose by oral gavage.

Rats were sacrificed at a predetermined time point of 10, 20, 30, 45, 60, 75, 100, 120, or 180 minutes after dosing. The intestines were removed, divided into the ten segments mentioned previously, and inspected for charcoal visually. The distance traveled by the charcoal plug was measured as the furthest point of the charcoal plug.

Dosing and sampling of amlodipine and glyburide

Rats (n=3) were intravenously administered a solution containing 2 mg/kg AML and 4 mg/kg GLY prepared in 50-55% NMP, 20% PEG-400, and 25-30% MiliQ water via the jugular cannula. Blood samples (~ 0.2 mL) were collected via the jugular cannula into heparinized tubes at 0.08, 0.25, 0.5, 1, 2, 4, 6, 8, 10, and 12 hours post-dose. Rats (n=3) were intravenously administered a solution containing 0.25 mg/kg DIG prepared in 15% NMP with saline via the jugular cannula. Blood samples (~ 0.2 mL) were collected via the jugular cannula into heparinized tubes at 0.08, 0.25, 0.5, 0.75, 1, 2, 4, 6, and 8 hours post-dose. After each sampling, the loss of blood volume was supplemented with an equal volume of saline containing 100 U/mL heparin. Blood samples were centrifuged at 5000 g for 15 minutes for AML and GLY or 10,000 g for 10 minutes for DIG at 4˚C to obtain plasma and kept at −20 °C until analysis.

Rats (n=13) were orally administered a solution containing 5 mg/kg AML and 5 mg/kg GLY in 50-55% NMP, 20% PEG-400, and 25-30% MiliQ water via oral gavage. While AML is not reported to be a transporter substrate, GLY absorption may be impacted by both uptake and efflux transporters. It is important to note that the use of 20% PEG-400 may alter efflux transporter activity toward GLY (Mudra and Borchardt, 2010), and this caveat was not further explored in the study. Rats were either fed (Fed, n=6), fasted 12 hours then fed 1 hour post-dose (Fasted- 1hr FT, n=4), or fasted 12 hours then fed 2 hours post-dose (Fasted- 2hr FT, n=3). Blood samples (~ 0.2 mL) were collected via the jugular cannula into heparinized tubes at 0.17, 0.5, 1, 1.5, 2.5, 4, 6, 8, 10, and 24 hours post-dose. Blood loss supplementation and plasma sample preparation were the same as that of the AML and GLY intravenous administration study.

Rats (n=14) were orally administered a solution containing 0.75 mg/kg DIG in 15% NMP in saline via oral gavage. Rats were either fed (Fed, n=5), fasted 12 hours then fed 0.5 hours post-dose (Fasted- 0.5hr FT, n=4), or fasted 12 hours then fed 1 hour post-dose (Fasted- 1hr FT, n=5). Blood samples (~ 0.2 mL) were collected via the jugular cannula into heparinized tubes at 0.08, 0.25, 0.5, 0.75, 1, 2, 4, 6, 8, and 24 hours post-dose. Blood loss supplementation and plasma sample preparation were the same as that of the DIG intravenous administration study.

Plasma samples for AML and GLY were mixed with two and a half times the volume of amlodipine-d4 (25 ng/mL) and glyburide-d3 (150 ng/mL) in acetonitrile as respective internal standards (IS). Samples were vortexed and centrifuged at 15,000 g for 10 minutes at 4˚C. Ten µL supernatant was injected into the LC-MS/MS system for analysis. DIG plasma samples were

mixed with two times the volume of digoxin-d3 in ACN. Samples were vortexed and centrifuged at 15,000 g for 10 minutes at 4˚C. Twenty µL supernatant was injected into the LC-MS/MS system for analysis.

Liquid chromatography tandem mass spectrometry

Analysis was performed using an Agilent series 1100 high-performance liquid chromatography (HPLC) system coupled to an ABSciex API 4000 triple-quadrupole tandem mass spectrometer with an electrospray ionization source. The mass spectrometer was operated in positive ion mode. All LC-MS/MS data were acquired and processed using Analyst software version 1.6.

Chromatographic separation for AML and GLY was performed on a Kinetex® C8 column (2.1 mm × 50 mm, 5 µm) protected by a Phenomenex Security Guard C18 (2.0 x 4 mm) guard column. The mobile phase for AML and GLY consisted of water with 0.1% formic acid (FA) as the aqueous phase (A) and ACN with 0.1% FA as the organic phase (B). The gradient started at 95% A and maintained for 1.3 minutes, ramped down to 0% over 30 seconds and held for 5.7 minutes, and then ramped back to 95% over 10 seconds and maintained until 9 minutes. The flow rate was 500 µL/min. The retention time for AML and AML-d4 was ~ 3.00 minutes, while the retention time for GLY and GLY-d3 was ~3.27 minutes. The precursor → product ion transitions observed for AML, AML-d4, GLY, and GLY-d3 were 409.2 → 237.3, 413.2 →237.3, 494.5 → 369.2, and 497.5 → 372.2, respectively.

For DIG, a Phenomenex® Gemini C18 column (100 mm × 4.6 mm, 3 µm) with a Phenomenex Security Guard C18 (2.0 x 4 mm) guard column was used. The mobile phase for DIG consisted of 10mM ammonium formate in water (pH to 4 with FA) as the aqueous phase (A) and ACN

with 0.1% FA as the organic phase (B). The gradient used for DIG elution started at 70% A and maintained for 1 minute, ramped down to 5% over 1.5 minutes and maintained for 2.5 minutes, and increasing back to 70% over 0.1 minutes for a total of 7 minutes. The flow rate was 600 μL/min. The retention time for DIG and DIG-d was ~4.54 minutes. The precursor → product ion transitions analyzed for DIG and DIGd3 were 798.5→651.5 and 801.5→654.5, respectively.

The dwell time for each ion transition was 200 msec. The operating parameters were optimized as follows: curtain gas, 20 psi; ion source gas 1, 60 psi; ion source gas 2, 40 psi; ion spray voltage, 5000 V; temperature, 500˚C. The declustering potential (DP), collection energy (CE), and collision cell exit potential (CXP) for AML are 71V, 17V, and 18V, respectively. The DP, CE, and CXP for GLY are 96V, 21V, and 19V, respectively. The DP, CE, and CXP for DIG are 70V, 20V, and 15V, respectively.

The combined method for AML and GLY was satisfactory for quantification over the range of 1.5 – 90 ng/mL and 25 – 1500 ng/mL for AML and GLY in rat plasma, respectively. The method for DIG was suitable for quantification from 0.75 – 96 ng/mL. The lower limit of quantitation (LLOQ) for AML, DIG, and GLY were 1.5 ng/mL, 0.75 ng/mL, and 25 ng/mL, respectively. The inter- and intraday percent accuracy and percent precision were within ±15% for all three drugs.

Compartmental modeling of IV datasets

Individual rat concentration-time profiles as well as naive-pooled average in each group upon IV dosing were used as inputs for compartmental modeling. Assuming linear pharmacokinetics at the doses used, standard compartmental models were used to fit the IV datasets. Modeling was conducted with Mathematica version 12.3.1 with 1/y weighting. Model selection was based on

AICc values, and the compartmental model fitted IV concentration-time profiles were used as disposition functions for the absorption model subsequently used for the oral datasets.

Intestinal model development

We have previously published in detail a human continuous absorption model (Nagar et al., 2017). The rat model described below used a similar framework, with key anatomical differences modeled as described below. This model predicts the fraction of drug absorbed and can predict bioavailability if first-pass metabolism data are available. The code for this model is provided in Supplementary Materials. The continuous absorption model is based on the basic convection-diffusion equation (Ni et al., 1980):

$$\frac{d}{dt}C(x,t) = D\frac{d^2}{dx^2}C(x,t) - \frac{Q}{\pi r^2}\frac{d}{dx}C(x,t) - \sum_{i=1}^{n} k_i C(x,t) \quad \text{Eq. 1}$$

where drug concentration (C) varies as a function of both distance (x) and time (t), D is the drug molecule diffusion coefficient, Q is the bulk fluid flow rate, r is the radius of the intestinal lumen, and k_i is the first-order rate constant for the *i*th radial transfer process. The first term describes axial diffusion, the spread of the drug pulse due to intestinal drug mixing, the second term describes convection, the axial bulk movement of the pulse, and the last term describes radial diffusion. This approach also includes relevant physiological and physicochemical factors.

For this model, the intestine is described as a continuous, concentric set of cylinders (Figure 1). In the axial direction, the drug enters as a plug from the stomach into the duodenum (10 cm), moves along the gut through the jejunum (106 cm), ileum (3 cm), and colon (16 cm) and stops at the terminal colon (Figure 1A). The model is velocity based ensuring that the plug is at the experimentally determined position over time. The small intestine is considered to have a

DMD Fast Forward. Published on March 26, 2022 as DOI: 10.1124/dmd.122.000831
This article has not been copyedited and formatted. The final version may differ from this version.

radius of 0.79 cm in the duodenum, 0.92 cm in the jejunum, 0.89 cm in the ileum, and 1.17 cm in the colon.

In the radial direction, this model includes an explicit enterocyte apical membrane, cytosol, and intercellular lipid compartments (Figure 1B). For absorption, the drug reversibly moves from the lumen (C1), through the apical enterocyte membrane (C2), into the enterocyte cytosol (C3), where it has the option to go into intracellular lipids (C4). In the final step, the drug irreversibly moves across the basolateral membrane into the portal blood (C5).

Physiologic functions: Expressions for relevant physiological parameters as functions of x were derived using combinations of logistic functions to match experimental data. These functions allowed for smooth transitions between intestinal segments and prevented mathematical discontinuities.

Velocity, vel(x). As the bulk pulse travels along the axial direction, it does so with a fluctuating velocity. Experimental time versus position data collected in-house were used to calculate experimental velocities as a function of x. The following expression for vel(x) was built using these velocities. Due to the absorption of luminal water and change in intestinal diameter, the velocity decreases along the small intestine, with the slowest velocity occurring in the colon. Equation 2 was used, and the profile and experimental velocity data are shown in Figure 2A.

$$vel(x) = \frac{a1}{a(x)}\left(2.4 - \frac{1.96}{1+e^{-20(-0.45+x)}} - \frac{0.19}{1+e^{-15(-1.05+x)}} - \frac{0.11}{1+e^{-25(-1.3+x)}} - \frac{0.09}{1+e^{-25(-1.399+x)}}\right.$$

Eq. 2

where a1 is the cross-sectional area at radius r_1 and a(x) is the cross-sectional area as a function of distance (x).

DMD Fast Forward. Published on March 26, 2022 as DOI: 10.1124/dmd.122.000831
This article has not been copyedited and formatted. The final version may differ from this version.

Effective diffusion, dif(x). Along with bulk axial movement, the drug pulse experiences effective axial diffusion. This axial spreading of the plug is greater than that expected by molecular diffusion and is likely due to peristalsis. Similar to the human model (Nagar et al., 2017), effective axial diffusion is a function of velocity, as shown in Equation 3 and Figure 2B.

$$dif(x) = 0.005\big(0.5 + 0.5\tan\big(75(x - .025)\big)\big)\, vel(x) \qquad \text{Eq. 3}$$

Cross-sectional area, a(x). The cross-sectional area is determined by the radii of each intestinal segment. The radii of the duodenum, jejunum, ileum, and colon are r_1, r_2, r_3, and r_4, respectively. Equation 4 was used, and the profile and experimental velocity data are shown in Figure 2C:

$$a(x) = a_1 + \frac{(a_2 - a_1)}{(1+e^{-25(x-0.15)})} + \frac{(a_3 - a_2)}{(1+e^{-20(x-jej5)})} + \frac{(a_4 - a_3)}{(1+e^{-75(x-ile)})} \qquad \text{Eq. 4}$$

where $a_1=\pi r_1^2$, $a_2=\pi r_2^2$, $a_3=\pi r_3^2$, $a_4=\pi r_4^2$, and jej5 = 1.16 m and ile = 1.19 m were used for distance to the end of the jejunum and ileum, respectively.

Surface area, sa(x).

The expressions for surface area per unit length (circumference) was based on experimental data collected in-house. The surface areas were determined by the radii and multiplication factors for villi and microvilli. The total surface area including microvilli and villi, $sa_{lumen}(x)$, is described in Equation 6 and the profile is shown in Figure 2D.

$$sa_{lumen}(x) = 0.472 + \frac{0.644}{(1+e^{-50(x-((0.05+duo)/2))})} - \frac{0.013}{(1+e^{-50(x-jej4)})} - \frac{0.488}{(1+e^{-50(x-jej5)})} - \frac{0.538}{(1+e^{-50(x-ile)})}$$

Eq. 5

DMD Fast Forward. Published on March 26, 2022 as DOI: 10.1124/dmd.122.000831
This article has not been copyedited and formatted. The final version may differ from this version.

where duo = 0.10 m, jej4 = 0.95 m, jej5 = 1.16 m, and ile = 1.19 m were used for distance to the end of the duodenum, fourth jejunal segment, the entire jejunum, and ileum, respectively.

The expansion factor for the increase in surface area due to microvilli alone, mf(x) is described in Equation 5 and the profile is shown in Figure 2E.

$$mf(x) = 9.2 + \frac{4.9}{(1+e^{-50(x-((0.05+duo)/2))})} + \frac{1.6}{(1+e^{-50(x-jej3)})} - \frac{9.1}{(1+e^{-25(x-ile)})} \quad \text{Eq. 6}$$

where duo = 0.10 m, jej3 = 0.74 m, and ile = 1.19 m were used for distance to the end of the duodenum, third jejunal segment, and ileum, respectively. The surface area without microvilli can then be calculated by $sa_{lumen}(x)/mf(x)$.

Cross-sectional area for the enterocyte apical membrane, $a_{mem}(x)$, cytosol, $a_{cyt}(x)$, and cytosolic lipid, $a_{lip}(x)$. The equations used to describe the cross-sectional area along the intestine for the enterocyte apical membrane, cytosol, and cytosolic lipids are described in more detail previously (Nagar et al., 2017) and are listed below.

$$a_{mem}(x) = (35 * 10^{-10})\, sa_{lumen}(x) \quad \text{Eq.7}$$

$$a_{cell}(x) = (20 * 10^{-6})\, sa_{villi}(x) \quad \text{Eq.8}$$

$$a_{lip}(x) = 15 * 10^{-7}\, sa_{villi}(x) \quad \text{Eq.9}$$

Where $sa_{villi}(x)$ equals $sa_{lumen}(x)/mf(x)$

pH of the intestines, pH(x). Fasted and fed pH data along the intestine was collected experimentally. The pH along the intestine under fasted conditions was described as a

DMD Fast Forward. Published on March 26, 2022 as DOI: 10.1124/dmd.122.000831
This article has not been copyedited and formatted. The final version may differ from this version.

combination of logistic functions expressed in Equation 10 and shown in Figure 2F. The pH along the intestine under fed conditions was described in Equation 11 and shown in Figure 2G.

$$pH_{fast}(x) = 6.5 - \frac{0.4}{1+e^{-75(-1.32+x)}} - \frac{1.2}{1+e^{-75(-1.25+x)}} + \frac{0.4}{1+e^{-50(-1.1+x)}} + \frac{0.7}{1+e^{-15(-1+x)}} + \frac{0.1}{1+e^{-.2(-.761+x)}}$$

Eq.10

$$pH_{fed}(x) = 6 + \frac{0.3}{1+e^{-30(-1.3+x)}} - \frac{2.1}{1+e^{-150(-1.25+x)}} + \frac{0.8}{1+e^{-50(-1.15+x)}} + \frac{0.7}{1+e^{-10(-.67+x)}} + \frac{0.3}{1+e^{-10(-.37+x)}} - \frac{0.1}{1+e^{-10(-.15+x)}}$$

Eq.11

Drug-specific functions:

Apparent Permeability, $P_{app}(x)$. For the current model, apparent permeability is based on Caco-2 cell permeability data and is modified by pH as described previously (Nagar et al., 2017). To account for species differences and the transition from *in vitro* to *in vivo*, a Caco-2 scaling factor of 1.2 was used. The equations for acids and bases were used were used for $P_{app}(x)$, respectively.

$$P_{app,a}(x) = \frac{P_{app,scaled}}{1+10^{ma/10(pH_C-pKa)}} * \frac{1}{1+10^{ma/10(pH(x)-pKa)}}$$

Eq.12

$$P_{app,b}(x) = \frac{P_{app,scaled}\left(1+10^{mb/10(pKa-pH(x))}\right)}{1+10^{mb/10(pKa-pH_C)}}$$

Eq.13

where $P_{app}(x)$ is the apparent permeability along the intestine, $P_{app,scaled}$ is the scaled Caco-2 permeability of a specific drug, ma is the slope of permeability versus pH for acids, and mb is the slope of permeability versus pH for bases, pH_C is the pH at which the Caco-2 experiments were conducted, pKa is the pKa for the drug, and pH(x) is the pH of the intestine at distance x. The pH(x) used was either $pH_{fast}(x)$ or $pH_{fed}(x)$, depending on the feeding condition of the animals.

DMD Fast Forward. Published on March 26, 2022 as DOI: 10.1124/dmd.122.000831
This article has not been copyedited and formatted. The final version may differ from this version.

Membrane Diffusional Clearances, $CL_i(x)$ and $CL_o(x)$. The movement of drug between compartments is described by diffusional clearances $CL_i(x)$ and $CL_o(x)$. Movement of drug into the membrane is the product of permeability and surface area:

$$CL_{i,1}(x) = 4P_{app}(x)\, sa_{lumen}(x) \quad \text{Eq. 14}$$

$$CL_{i,2}(x) = 4P_{app2}(x)\, sa_{lumen}(x) \quad \text{Eq. 15}$$

$$CL_{i,3}(x) = 4P_{app}(x)\, 100\, sa_{lumen}(x) \quad \text{Eq. 16}$$

where $CL_{i,2}(x)$ is the diffusional clearance when radial diffusion is the rate-limiting step and $CL_{i,3}(x)$ is the diffusional clearance for the intracellular lipid compartment, by accounting for the difference in the surface area between the plasma membrane and intracellular lipids (1% plasma membrane). P_{app2} is the modified apparent permeability when radial diffusion is the rate-limiting step and is modified by a radial diffusion function (Equation 18) to slow radial diffusion as the pulse approaches the end of the colon:

$$P_{app2}(x) = \frac{P_{app}(x) f_{raddif}(x)}{P_{app}(x) + f_{raddif}(x)} \quad \text{Eq. 17}$$

$$f_{raddif}(x) = 0.005(1 - \tanh 75(x - 1.38)) \quad \text{Eq. 18}$$

The diffusional clearance out of membranes, $CL_o(x)$, is dependent on membrane partitioning (Korzekwa et al., 2012). Therefore, radial diffusion out of the membranes (Equation 19) and membrane partitioning (Equation 20) can be explained by the following equations:

$$Cl_o(x) = Cl_i(x) / K_p \quad \text{Eq. 19}$$

$$K_p = \frac{1 - f_{um}}{0.0007 f_{um}} \quad \text{Eq. 20}$$

DMD Fast Forward. Published on March 26, 2022 as DOI: 10.1124/dmd.122.000831
This article has not been copyedited and formatted. The final version may differ from this version.

where f_{um} is the fraction unbound in microsomes.

Transporter Expression for Pgp and Oatp2b1, Pgp(x) and Oatp(X). To simulate the impact of transporters P-gp and Oatp2b1 reported transporter levels were used (MacLean et al., 2010; Mai et al., 2021). Transporter expression use and normalization was performed in the same manner as that described previously (Nagar et al., 2017). The P-gp and normalized Oatp2b1 expression functions are shown in Figure 2H and 2I, respectively. This led to the development of Michaelis-Menten saturation functions:

$$\frac{d}{dt}C1(x,t) = \frac{-V_{m,Oatp}(x)\ C1(x,t)}{\left(K_{m,Oatp}+C1(x,t)\right)a(x)} + \frac{V_{m,Pgp}(x)\ C2(x,t)}{\left(K_{m,Pgp}+C2(x,t)\right)a(x)} \quad \text{Eq. 21}$$

$$\frac{d}{dt}C2(x,t) = \frac{-V_{m,Pgp}(x)\ C2(x,t)}{\left(K_{m,Pgp}+C2(x,t)\right)a_{mem}(x)} \quad \text{Eq. 22}$$

$$\frac{d}{dt}C3(x,t) = \frac{V_{m,Oatp}(x)\ C1(x,t)}{\left(K_{m,Oatp}+C1(x,t)\right)a_{cell}(x)} \quad \text{Eq. 23}$$

where

$$V_{m,Oatp}(x) = \frac{10\ 000 f_{raddif}(x)\ F_{Oatp}\ Oatp(x)}{10\ 000 f_{raddif}(x) + F_{Oatp}\ Oatp(x)} \quad \text{Eq. 24}$$

$$Oatp(x) = 1.6 + \frac{4.4}{(1+e^{-50(x-0.1)})} + \frac{2}{(1+e^{-15(x-0.9)})} + \frac{2}{(1+e^{-50(x-1.275)})} \quad \text{Eq. 25}$$

$$V_{m,Pgp}(x) = F_{Pgp}\ Pgp(x) \quad \text{Eq. 26}$$

$$Pgp(x) = 2.08 + \frac{1.15}{(1+e^{-12(x-0.4)})} + \frac{0.49}{(1+e^{-10(x-0.9)})} + \frac{1.45}{(1+e^{-55(x-1.25)})} \quad \text{Eq. 27}$$

To make radial diffusion rate limiting for luminal uptake in the descending colon, the radial diffusion function, $f_{raddif}(x)$ was used. F_{Oatp} and F_{Pgp} are the factors to convert transporter per mg

mucosal tissue to mg drug transported per hour per unit volume of lumen for Oatp and apical membrane for Pgp, respectively.

DIG is known to be a Pgp substrate, while GLY relies on both Oatp and Pgp (El-Kattan and Varma, 2011; Estudante et al., 2013; Suzuki et al., 2014). Presence of food is reported to inhibit Oatp2b1, leading to PK differences between fasted and fed groups (Lee et al., 2020). The following empirical values, based upon preliminary optimization steps using the observed data, were used for transporter functions for DIG (Pgp) and GLY (Pgp and Oatp).

For DIG, $K_{m,Pgp}$ = 9,000 µM and F_{Pgp} =150 for all groups. For GLY, $K_{m,Pgp}$ = 50 µM and F_{Pgp} = 5000 for all groups. GLY Fasted- 2hr FT and Fasted- 1hr FT groups used a $K_{m,Oatp}$ = 5 µM, while the fed group used a $K_{m,Oatp}$ = 50 µM. Fasted- 2hr FT group used F_{Oatp} = 3.5, while the Fasted- 1hr FT and fed group used a F_{Oatp} = 0.2. Thus, Oatp activity had to be reduced for GLY datasets when food was present.

Solution dosing input and disposition equations:

From in vivo data with different feeding times post dose, it is apparent that 1) some of the oral dose is immediately available for absorption, 2) feeding results in delayed release into the intestine, and 3) the longer the time before feeding, less of the dose is retained. Therefore, drug input from the stomach was modeled by three unit pulse functions with a lag time (Figure 3). The first pulse represents 10% of the dose that immediately enters the intestine, the second pulse represents the drug that is released into the intestine in the fasted state post-dose, and the third pulse is the remaining dose released over a 20h period in the presence of food. The unit pulse functions for the three pulses are:

DMD Fast Forward. Published on March 26, 2022 as DOI: 10.1124/dmd.122.000831
This article has not been copyedited and formatted. The final version may differ from this version.

$$upulse_1(t) = 0.5\,(\tan[300(t - lag)] - \tan[50(t - (PL_{t1} + lag))]) \quad \text{Eq. 28}$$

$$upulse_2(t) = 0.5\,(\tan[300(t - lag)] - \tan[50(t - (PL_{t2} + lag))]) \quad \text{Eq. 29}$$

$$upulse_3(t) = 0.5\,(\tan[300(t - (PL_{t1} + lag))] - \tan[100(t - (PL_{t2} + PL_{t3} + lag))])$$

Eq. 30

where lag = 0.1 hr, PL_{t1} = 0.1 hr, PL_{t2} = FT, and PL_{t3} = 20 hr, FT is the time food was reintroduced to animals after dosing drug. For fed animals, PL_{t2} = 0.001 hr was used.

The appropriate initial concentration and velocity in the duodenum was achieved by multiplying the upulse functions by the dosing concentration and a volume correction factor:

$$pulse_i(t) = C_0 * V_{corr,i} * upulse_i(t) \quad \text{Eq. 31}$$

where C_0 = dose/ $V_{s,o}$ mg/mL, and $V_{s,o}$ is the volume of water introduced into the stomach with the drug (1ml/kg). The V_{corr} term is the volume correction factor for each pulse necessary to achieve the correct velocity entering the intestine:

$$V_{corr,1} = \frac{0.1\,V_{s,o}}{PL_{t1} * \pi * {r_1}^2 * Vel0} \quad \text{Eq. 32}$$

$$V_{corr,2} = \frac{0.9\,V_{s,o}\,(\frac{PL_{t2}}{2.5})}{PL_{t2} * \pi * {r_1}^2 * Vel0} \quad \text{Eq. 33}$$

$$V_{corr,3} = \frac{0.9\,V_{s,o}\,(\frac{2.5 - PL_{t2}}{2.5})}{PL_{t3} * \pi * {r_1}^2 * Vel0} \quad \text{Eq. 34}$$

where Vel0 is the velocity at x=0.

DMD Fast Forward. Published on March 26, 2022 as DOI: 10.1124/dmd.122.000831
This article has not been copyedited and formatted. The final version may differ from this version.

Drug solution disposition in the rat intestine was modeled for drug concentrations in the lumen, C1(x,t), apical membrane, C2(x,t), enterocyte cytosol, C3(x,t), and optional partitioning into intracellular lipids, C4(x,t), with the following PDEs:

$$\frac{d}{dt}C1(x,t) = dif(x)\frac{d^2}{dx^2}C1(x,t) + \left(-vel(x) + \frac{d}{dx}dif(x) + \frac{dif(x)}{a(x)}\frac{d}{dx}a(x)\right)\frac{d}{dx}C1 + \left(-\frac{d}{dx}vel(x) - \frac{vel(x)}{a(x)}\frac{d}{dx}a(x)\right)C1(x,t) - \frac{Cl_{i,2}(x)}{a(x)}C1(x,t) + \frac{Cl_{o,2}(x)}{a(x)}C2(x,t) - \frac{V_{m,Oatp}\,C1(x,t)}{(K_{m,Oatp}+C1(x,t))a_{mem}(x)} + \frac{V_{m,Pgp}\,C2(x,t)}{(K_{m,Pgp}+C2(x,t))a_{mem}(x)} \quad \text{Eq. 35}$$

$$\frac{d}{dt}C2(x,t) = \frac{Cl_{i,2}(x)}{a_{mem}(x)}C1(x,t) - \left(\frac{Cl_{o,1}(x)+Cl_{o,2}(x)}{a_{mem}(x)}\right)C2(x,t) + \frac{Cl_{i,1}(x)}{a_{mem}(x)}C3(x,t) - \frac{V_{m,Pgp}\,C2(x,t)}{(K_{m,Pgp}+C2(x,t))a_{mem}(x)} \quad \text{Eq. 36}$$

$$\frac{d}{dt}C3(x,t) = \frac{Cl_{o,1}(x)}{a_{cell}(x)}C2(x,t) - \frac{Cl_{i,1}(x)}{a_{cell}(x)}C3(x,t) - \frac{Cl_{i,1}(x)}{2a_{cell}(x)}C3(x,t) - \frac{Cl_{i,3}(x)}{a_{cell}(x)}C3(x,t) + \frac{Cl_{o,3}(x)}{a_{cell}(x)}C4(x,t) + \frac{V_{m,Oatp}\,C1(x,t)}{(K_{m,Oatp}+C1(x,t))a_{mem}(x)} \quad \text{Eq. 37}$$

$$\frac{d}{dt}C4(x,t) = \frac{Cl_{i,3}(x)}{a_{lip}(x)}C3(x,t) - \frac{Cl_{0,3}(x)}{a_{lip}(x)}C4(x,t) \quad \text{Eq. 38}$$

with initial conditions, C1(t, 0) = $pulse_1$(t) + $pulse_2$(t) + $pulse_3$(t),

C1(0, x) = $C_{1,0}$ (where $C_{1,0}$ is defined as the concentration of $pulse_1$(t) at t = 0),

C1(t, 1.45) = 0, C2(0, x) = 0, C2(t, 0) = 0, C2(t, 1.45) = 0, C3(0, x) = 0, C3(t, 0) = 0, C3(t, 1.45) = 0, C4(t, 0) = 0, C4(0, x) = 0, C4(t, 1.45) = 0.

Systemic PK and disposition functions:

The movement of drug from the enterocyte cytosol into the systemic PK model was modeled by the input function:

$$Inputf(t) = \int_{x=0}^{x=1.45} \frac{CL_i(x)}{2} C3(x,t) \quad \text{Eq. 39}$$

The systematic disposition functions were generated from experimentally collected IV data model by 2-compartmental PK models. The systemic disposition functions were combined with the input function (Eq. 32) to simulate oral PK profiles.

Methods for numerical solutions:

All models were developed using Mathematica 12.3.1. IV data were fit using a NonLinearModelFit with a PrecisionGoal → Infinity and 1/Y weighting. ODEs and PDEs were simulated using the NDSolve function. PDEs were solved using the method of lines with default step sizes, SpatialDiscretization → TensorProductGrid, DifferenceOrder →2, and grid x-coordinates defined as follows:

$$\text{coordx} =$$
$$\text{Join}[0 + \text{Range}[0, 60]/400\,, 0.15 + \text{Range}[1, 250]/1000\,, 0.4 + \text{Range}[1, 200]/1000\,, 0.6 + \text{Range}[1, 45]/300\,, 0.75 + \text{Range}[1, 700]/1000] \quad \text{Eq. 40}$$

Input and experimental data:

Permeability data from Caco-2 cells were obtained from the literature (Table 1). An exposure overlap coefficient (EOC) (Holt et al., 2019) was calculated to compare the simulated C-t profiles to the experimental oral PK profiles. An interpolation function was generated from the experimental oral C-t data (Interpolation function in Mathematica with Method → Spline and InterpolationOrder → 1). Since experimental clearances were used, the simulated C-t profile was

normalized to have the same AUC as the experimental profile. The overlap AUC was obtained by integrating the minimum of the two C-t functions. Lastly, the EOC was calculated as the overlap AUC/experimental AUC. The value of the EOC ranges between zero, no overlap, and one, complete overlap.

Results

Rat intestinal measurements

Dimensions of the rat intestine were measured experimentally and utilized to develop the intestinal model (Figure 1A). Figure 2 shows the in-house generated velocity, cross-sectional surface area, fasted pH, and fed pH along the length of the rat intestine. In fed rats, the pH began at ~6 in the duodenum and gradually increased to ~7.5 in the ileum. The pH rapidly decreased to ~5.5 in the cecum, where it remained until the distal colon (Figure 2G). In fasted rats, the pH started higher at ~6.5 in the duodenum and was maintained until the J4 segment. The pH in the ileum of fasted rats matched that of the fed group at ~7.5 before decreasing back to ~6.5 in the cecum and gradually declining along the colon (Figure 2F). The fasted group had a significantly higher pH in the duodenum, J1, J2, cecum, and proximal colon segments (see Supplementary Materials, Table S1).

In both fed and fasted states, the velocity decreased as the charcoal plug moved along the intestine from the duodenum to the ileum (see Supplementary Materials, Tables S2 and S3). There was no statistically significant difference in the position versus time data between fasted and fed rats, so a single average velocity function was calculated and used to describe vel(x) (Figure 2A).

Pharmacokinetics of AML, DIG, and GLY after IV and oral administration

The individual and naïve pooled average rat (n=3) IV data for AML, DIG, and GLY were best described by a 2-compartment model and are shown in Figure 4A, 5A, and 6A, respectively. The parameter estimates and metrics for the naïve pooled average datasets for all three drugs upon a single IV bolus dose are listed in Table 2.

The individual and naïve pooled average rat oral data for AML are shown in Figure 4. The observed Cmax and tmax values for the Fasted- 2hr FT, Fasted- 01hr FT, and Fed groups are listed in Table 3. The tmax for the Fed group was 21.8 hrs and was statistically different from the fasted groups ($p = 0.02$ with one-way ANOVA and posthoc Tukey's HSD test). The individual and naïve pooled average rat oral data for DIG are shown in Figure 5, and the observed Cmax and tmax values for the Fasted- 1hr FT, Fasted- 0.5hr FT, and Fed group are listed in Table 3. The individual and naïve pooled average rat oral data for GLY are shown in Figure 6, and the observed Cmax and tmax values for the Fasted- 2hr FT, Fasted- 1hr FT, and Fed group are in Table 3. There was no significant difference in Cmax and tmax values among the DIG and GLY groups. The inter-animal variability for all DIG and GLY PO groups was large, and may have contributed to poor prediction with the mean datasets (see Figure 7).

Prediction of absorption with the continuous absorption model

Figure 7 shows observed and predicted C-t profiles for three drugs dosed in solution under different feeding conditions. The predicted curves were normalized to the observed AUC, by optimizing the first-pass metabolism (FgFh) value to obtain the experimental AUC. Therefore, only the rate of absorption and shape of the C-t profiles were predicted (see Table 3 for predicted Cmax and tmax). The areas in green represent the overlap between the observed and predicted C-t profiles. The numerical values of the EOCs along with experimental and predicted Cmax and tmax are listed in Table 3. The AML Cmax and tmax predictions across the groups were in good agreement with the observed data. For DIG and GLY, the predicted tmax values were longer than mean observed values for all groups (Figure 7 and Table 3). Overall, the shape of the C-t profilesfor all three drugs was generally well predicted under all three feeding conditions with EOC values ranging from 0.80 to 0.97.

Discussion

The goals of this work were to i) develop a continuous rat intestinal absorption model and ii) to develop a modeling framework for prediction of food effects in oral drug absorption. We specifically aimed to study the impact of feeding time on oral drug absorption for three model drugs in a rat model. Utilizing the previously published human continuous intestinal absorption model, a rodent model was developed using species specific physiologic parameters as a function of length x. The inclusion of an explicit membrane compartment allowed for accurate modeling of the efflux transporter Pgp and membrane partitioning, while the inclusion of an intracellular lipid compartment allowed for modeling of lipid partitioning. The rat intestinal model was built based on in-house experimental measurements of intestinal dimensions, velocity, and pH. Novel aspects of the work include the following characteristics in a continuous intestinal model: i) inclusion of experimentally measured fasted and fed intestinal pH profiles, ii) inclusion of an experimentally measured velocity function, iii) inclusion of efflux and uptake transporter expression data, and iv) development of input functions based on experimental fasting and feeding times to recapitulate differences in stomach emptying in the presence of food.

While rodent models are useful for proof-of-concept exploration, they may not be useful to scale up complex oral absorption processes to man. The most notable species differences are the structure of the stomach and the composition of the intestine. The human stomach is a single gastric compartment, while the rodent stomach is both glandular, which contains glands that secrete gastric acid, and non-glandular. A limiting ridge, a thickened portion of lamina propria, separates these portions (Kararli, 1995; DeSesso and Jacobson, 2001). This limiting ridge and dual-portioned stomach may account for why food is present in the rat stomach after a 12 hour fast while the human stomach is over 90% empty after only 4 hours of fasting (Read et al., 1986;

Jeffrey et al., 1987). Also, the duodenum, jejunum, and ileum make up 4%, 38%, and 58% of the small intestine respectively in humans and 8%, 90%, and 2% of the small intestine in rats. Additionally, the cecum is 26% of the length of the large intestine in rats but is only 5% in humans (Kararli, 1995; Vdoviakova et al., 2016). Humans have three enlargement factors that contribute to the increased absorptive surface area, Kerckring's folds, villi, and microvilli while rats lack Kerckring's folds. While humans and rats have a similar pH range (~ 6 – 8) and trend along the intestine, humans have a gastric pH around 1 – 2.5, while rats have a more alkaline gastric pH around 3 – 4 (Ward and Coates, 1987; Evans et al., 1988). Humans have two primary intestinal uptake transporters, OATP1A2 and OATP2B1, while rats have several (Suzuki et al., 2012; Takeda et al., 2021). Rats have two mdr1 genes, mdr1a and mdr1b, while humans only have one MDR1 gene. For both species, the protein expression of P-gp increases from the proximal to distal regions (Brady et al., 2002). Lastly, rats do not possess a gallbladder, which stores and releases concentrated bile in humans when food is present. Bile salts can increase the dissolution rate and solubility of lipophilic compounds, aiding in their intestinal absorption (Kararli, 1995).

The factors stated above can additionally contribute to vast inter-animal variability in rat oral absorption profiles. It has been documented that rats with the same dosing conditions (same compound, dose, route of administration, formulation, dosing regimen, and feeding) exhibit AUC ratios of greater than 2 (Daublain et al., 2017). Along with distinctive physiological factors, feeding regimens, including volume and frequency of food consumption could introduce variability. Animals given food *ad libitum* will have variable self-imposed feeding regimens. Even when food is removed from the cages of rats in fasted groups, rats are known to eat anything available to them, including their bedding and engaging in coprophagy. The present

studies were not conducted using metabolic cages, and these factors may have contributed to lack of differences in transit times between fasted and fed groups in GI motility studies (see Supplementary Material, Tables S2 and S3).

Incorporating the ability to model various aspects of food effects to predict PK of oral drugs is important (Lin and Wong, 2017). The ACAT model allows for the modeling of food effects by varying physiological parameters that influence drug absorption, such as gastric pH and emptying time along with bile salt concentrations (Cheng and Wong, 2020). PBPK software built with compartmental absorption models have the capability to evaluate various food effects. PBPK modeling was used to discern that oral absorption of delayed-release zolpidem depended on the formulation in the fasted state, but depended on gastric emptying in the fed state (Andreas et al., 2017). The impact of food on drug solubility and resulting oral absorption was evaluated with a PBPK modeling software in another study (Zhang et al., 2014). The present work focused on evaluating the impact of feeding time on oral absorption. While human studies usually detail fasting and post-dosing feeding times, these details are not provided in preclinical oral dosing studies. This work illustrates the critical need to document and model appropriately the absence and presence of food, including feeding time, in oral dosing studies. The rat continuous intestinal absorption model developed here included separate intestinal pH functions for fasted and fed conditions (Figure 2). In addition, we developed a drug input function that accounted for the introduction of food post-dosing (Figure 3). The drug input function was based on experimental design (Figure 3A), as well as the observed slower slope of the terminal C-t profiles upon oral dosing when compared with the IV C-t profiles (Figures 4 - 6), indicating that absorption was occurring even at later time-points. Delayed absorption in the presence of standard or high fat food has been reported for several BCS class 1 – 4 drugs in humans (Deng et al., 2017). With the

input functions incorporating impact of feeding time, the continuous absorption model predicted with marked accuracy the observed mean C-t profiles for all groups for the 3 drugs tested (Figure 7). These results indicate the utility of the modeling framework to evaluate the impact of feeding time on oral absorption.

As with the compartmental PBPK software, active transport is easily incorporated into the continuous absorption model. DIG is a well-known substrate of Pgp and inhibition of this transporter has been shown to increase the AUC of DIG in rats (Suzuki et al., 2014). Predictions of DIG using only a passive permeability model overpredicted the Cmax in both fasted groups (data not shown). The addition of Pgp improved the accuracy of C-t predictions for DIG. For GLY, a known transporter substrate for both Pgp and Oatp (El-Kattan and Varma, 2011; Estudante et al., 2013), improved predictions were obtained when transporters were added. It was interesting that reduced Oatp activity had to be used for groups in the presence of food, which aligns with the observed Oatp inhibition in the presence of food (Lee et al., 2020).

The present work includes studies with three drugs as proof of concept. The continuous absorption model is not a validated model, and its use for predicting oral absorption of a variety of small molecules will be necessary for validation in the future. Refinements to the model and to the input function will likely be necessary, to include complexities such as type of food, formulation-food interactions, and acute drug-food interactions. The rat model is not intended for eventual scaling to humans, but instead to provide a species-specific framework to evaluate complexities including a wide variety of food effects on oral absorption. Work is currently underway to use this rat model to evaluate the impact of formulation design on oral absorption. Additionally, we are incorporating gut metabolism into the model. A similar model for the mouse is currently under development in our lab and is expected to provide additional insights

into oral absorption in the presence and absence of drug metabolizing enzymes and transporters, and with a variety of formulations. Together, this work will advance refinement of the original human continuous absorption model in a species-specific manner and will broadly provide mathematical tools to evaluate various types of food and formulation effects on oral drug absorption across species. It is hoped that the code provided for this model will encourage others to refine, incorporate additional intestinal/drug features, and validate this framework.

Authorship Contributions

Participated in research design: Radice C, Korzekwa K, Nagar S

Conducted experiments: Radice C

Performed data analysis: Radice C, Korzekwa K, Nagar S

Wrote or contributed to the writing of the manuscript: Radice C, Korzekwa K, Nagar S

References

Alqahtani MS, Kazi M, Alsenaidy MA, and Ahmad MZ (2021) Advances in Oral Drug Delivery. *Frontiers in Pharmacology* **12**.

Andreas CJ, Pepin X, Markopoulos C, Vertzoni M, Reppas C, and Dressman JB (2017) Mechanistic investigation of the negative food effect of modified release zolpidem. *Eur J Pharm Sci* **102:**284-298.

Brady JM, Cherrington NJ, Hartley DP, Buist SC, Li N, and Klaassen CD (2002) Tissue distribution and chemical induction of multiple drug resistance genes in rats. *Drug Metab Dispos* **30:**838-844.

Cao XH, Gibbs ST, Fang LY, Miller HA, Landowski CP, Shin HC, Lennernas H, Zhong YQ, Amidon GL, Yu LX, and Sun DX (2006) Why is it challenging to predict intestinal drug absorption and oral bioavailability in human using rat model. *Pharm Res* **23:**1675-1686.

Cheng LS and Wong H (2020) Food Effects on Oral Drug Absorption: Application of Physiologically-Based Pharmacokinetic Modeling as a Predictive Tool. *Pharmaceutics* **12**.

Daublain P, Feng KI, Altman MD, Martin I, Mukherjee S, Nofsinger R, Northrup AB, Tschirret-Guth R, Cartwright M, and McGregor C (2017) Analyzing the Potential Root Causes of Variability of Pharmacokinetics in Preclinical Species. *Mol Pharm* **14:**1634-1645.

Deng J, Zhu X, Chen Z, Fan CH, Kwan HS, Wong CH, Shek KY, Zuo Z, and Lam TN (2017) A Review of Food-Drug Interactions on Oral Drug Absorption. *Drugs* **77:**1833-1855.

DeSesso JM and Jacobson CF (2001) Anatomical and physiological parameters affecting gastrointestinal absorption in humans and rats. *Food Chem Toxicol* **39:**209-228.

Djuv A and Nilsen OG (2008) Caco-2 cell methodology and inhibition of the P-glycoprotein transport of digoxin by Aloe vera juice. *Phytother Res* **22:**1623-1628.

Dou L, Mai Y, Madla CM, Orlu M, and Basit AW (2018) P-glycoprotein expression in the gastrointestinal tract of male and female rats is influenced differently by food. *Eur J Pharm Sci* **123:**569-575.

El-Kattan A and Varma M (2011) Oral Absorption, Intestinal Metabolism and Human Oral Bioavailability, in: *Topics on Drug Metabolism*.

Estudante M, Morais JG, Soveral G, and Benet LZ (2013) Intestinal drug transporters: An overview. *Adv Drug Deliv Rev* **65:**1340-1356.

Evans DF, Pye G, Bramley R, Clark AG, Dyson TJ, and Hardcastle JD (1988) Measurement of gastrointestinal pH profiles in normal ambulant human-subjects *Gut* **29:**1035-1041.

Higashi K, Tanaka C, Imanishi K, Sawamoto K, Horikawa T, Ohkawa H, Matsushita R, Sai Y, and Miyamoto K (2013) Influence of long-term enteral nutrition on pharmacokinetics of digoxin in rats. *Drug Metab Pharmacokinet* **28:**44-52.

Holt K, Ye M, Nagar S, and Korzekwa K (2019) Prediction of Tissue-Plasma Partition Coefficients Using Microsomal Partitioning: Incorporation into Physiologically based Pharmacokinetic Models and Steady-State Volume of Distribution Predictions. *Drug Metab Dispos* **47:**1050-1060.

Huang WL, Lee SL, and Yu LX (2009) Mechanistic Approaches to Predicting Oral Drug Absorption. *Aaps J* **11:**217-224.

Jeffrey P, Burrows M, and Bye A (1987) Does the rat have an empty stomach after an overnight fast? *Lab Anim* **21:**330-334.

Jiang SW, Zhao WM, Chen Y, Zhong ZY, Zhang MA, Li F, Xu P, Zhao KJ, Li Y, Liu L, and Liu XD (2015) Paroxetine decreased plasma exposure of glyburide partly via inhibiting intestinal absorption in rats. *Drug Metab Pharmacokinet* **30:**240-246.

Kararli TT (1995) Comparison of the gastrointestinal anatomy, physiology, and biochemistry of humans and commonly used laboratory-animals *Biopharm Drug Dispos* **16:**351-380.

Klein S (2010) The Use of Biorelevant Dissolution Media to Forecast the In Vivo Performance of a Drug. *Aaps J* **12:**397-406.

Korzekwa KR, Nagar S, Tucker J, Weiskircher EA, Bhoopathy S, and Hidalgo IJ (2012) Models to Predict Unbound Intracellular Drug Concentrations in the Presence of Transporters. *Drug Metab Dispos* **40:**865-876.

Lee W, Ha JM, and Sugiyama Y (2020) Post-translational regulation of the major drug transporters in the families of organic anion transporters and organic anion-transporting polypeptides. *Journal of Biological Chemistry* **295:**17349-17364.

Li Y, Wei Y, Zhang F, Wang D, and Wu X (2012) Changes in the pharmacokinetics of glibenclamide in rats with streptozotocin-induced diabetes mellitus. *Acta Pharmaceutica Sinica B* **2:**198-204.

Lin L and Wong H (2017) Predicting Oral Drug Absorption: Mini Review on Physiologically-Based Pharmacokinetic Models. *Pharmaceutics* **9:**14.

MacLean C, Moenning U, Reichel A, and Fricker G (2010) Regional absorption of fexofenadine in rat intestine. *Eur J Pharm Sci* **41:**670-674.

Mai Y, Dou L, Yao ZC, Madla CM, Gavins FKH, Taherali F, Yin HY, Orlu M, Murdan S, and Basit AW (2021) Quantification of P-Glycoprotein in the Gastrointestinal Tract of Humans and Rodents: Methodology, Gut Region, Sex, and Species Matter. *Mol Pharm* **18:**1895-1904.

Melander A (1978) Influence of food on the bioavailability of drugs. *Clinical Pharmacokinetics* **3:**337-351.

Mudra DR and Borchardt RT (2010) Absorption barriers in the rat intestinal mucosa. 3: Effects of polyethoxylated solubilizing agents on drug permeation and metabolism. *J Pharm Sci* **99:**1016-1027.

Nagar S and Korzekwa K (2017) Drug Distribution. Part 1. Models to Predict Membrane Partitioning. *Pharm Res* **34:**535-543.

Nagar S, Korzekwa RC, and Korzekwa K (2017) Continuous Intestinal Absorption Model Based on the Convection-Diffusion Equation. *Mol Pharm* **14:**3069-3086.

Ni PF, Ho NFH, Fox JL, Leuenberger H, and Higuchi WI (1980) Theoretical model studies of intestinal drug absorption V. Non-steady-state fluid flow and absorption. *International Journal of Pharmaceutics* **5:**33-47.

Owens K, Argon S, Yu J, Yang X, Wu F, Lee SC, Sun WJ, Ramamoorthy A, Zhang L, and Ragueneau-Majlessi I (2021) Exploring the Relationship of Drug BCS Classification, Food Effect, and Gastric pH-Dependent Drug Interactions. *AAPS J* **24:**16.

Read NW, Aljanabi MN, Holgate AM, Barber DC, and Edwards CA (1986) Simultaneous measurement of gastric-emptying, small-bowl residence and colonic filling of a solid meal by the use of the gamma-camera *Gut* **27:**300-308.

Singh RP, Sabarinath S, Gautam N, Gupta RC, and Singh SK (2011) Pharmacokinetic study of the novel, synthetic trioxane antimalarial compound 97-78 in rats using an LC-MS/MS method for quantification. *Arzneimittelforschung-Drug Res* **61:**120-125.

Small DS, Zhang W, Royalty J, Cannady EA, Downs D, Friedrich S, and Suico JG (2015) A Multidose Study to Examine the Effect of Food on Evacetrapib Exposure at Steady State. *J Cardiovasc Pharmacol Ther* **20:**483-489.

Stader F, Kinvig H, Penny MA, Battegay M, Siccardi M, and Marzolini C (2020) Physiologically Based Pharmacokinetic Modelling to Identify Pharmacokinetic Parameters Driving Drug Exposure Changes in the Elderly. *Clin Pharmacokinet* **59:**383-401.

Suzuki K, Shitara Y, Fukuda K, and Horie T (2012) Long-Lasting Inhibition of the Intestinal Absorption of Fexofenadine by Cyclosporin a in Rats. *Journal of Pharmaceutical Sciences* **101:**2606-2615.

Suzuki M, Komura H, Yoshikawa T, Enya S, Nagao A, Takubo H, and Kogayu M (2014) Characterization of gastrointestinal absorption of digoxin involving influx and efflux transporter in rats: application of mdr1a knockout (-/-) rats into absorption study of multiple transporter substrate. *Xenobiotica* **44:**1039-1045.

Takeda F, Oda M, Terasaki M, Kubota A, Asada K, Ichimura Y, Kojima H, and Saitoh H (2021) Downregulated expression of organic anion transporting polypeptide (Oatp) 2b1 in the small intestine of rats with acute kidney injury. *Drug Metab Pharmacokinet* **40:**1-9.

Varma MV, Scialis RJ, Lin J, Bi YA, Rotter CJ, Goosen TC, and Yang X (2014) Mechanism-based pharmacokinetic modeling to evaluate transporter-enzyme interplay in drug interactions and pharmacogenetics of glyburide. *AAPS J* **16:**736-748.

Vdoviakova K, Petrovova E, Maloveska M, Kresakova L, Teleky J, Elias MZJ, and Petrasova D (2016) Surgical Anatomy of the Gastrointestinal Tract and Its Vasculature in the Laboratory Rat. *Gastroenterol Res Pract***:**11.

Vermeulen JK, Vries AD, Schlingmann F, and Remie R (1997) Food deprivation: common sense or nonsense? *Animal Technology* **48**.

Ward FW and Coates ME (1987) Gastrointestinal pH measurement in rats - influence of the microbial-flora, diet and fasting *Lab Anim* **21:**216-222.

Welling PG (1977) Influence of food and diet on gastrointestinal drug absorption: a review. *J Pharmacokinet Biopharm* **5:**291-334.

Zhang H, Xia B, Sheng J, Heimbach T, Lin TH, He H, Wang Y, Novick S, and Comfort A (2014) Application of physiologically based absorption modeling to formulation development of a low solubility, low permeability weak base: mechanistic investigation of food effect. *AAPS PharmSciTech* **15:**400-406.

Footnote

This work was supported by the National Institutes of Health National Institute of General Medical Sciences (to S.N. and K.K.) [Grants 2R01GM104178 and 2R01GM114369].

Financial Disclosure and Conflict of Interest: The authors have no financial disclosures, and no conflicts of interest to report.

Figure legends

Figure 1. Rat continuous intestinal absorption model. A) Depiction of the rat intestine as a continuous cylinder. Duo: duodenum, Jej: jejunum, Ile: ileum, r1: radius of Duo, r2: radius of Jej, r3: radius of Ile, and r4: radius of the colon. B) Depiction of the radial compartments comprising the concentric cylinders of the rat intestine. Compartments C1 – C5 are defined as follows. C1: lumen; C2: apical membrane; C3: enterocyte cytosol; C4: intracellular lipid; C5: portal blood. Diffusional clearances into (CL_i) and out of (CL_o) membranes are as defined in Methods.

Figure 2. Physiological functions describing the intestine. Functions along distance x are shown for A) velocity, vel(x), B) effective diffusion, dif(x), C) cross-sectional area, a(x), D) surface area with villi and microvilli, $sa_{lumen}(x)$, E) microvilli expansion factor, mf(x), F) fasted intestinal pH, $pH_{fast}(x)$, G) fed intestinal pH, $pH_{fed}(x)$, H) P-gp pmol/mg tissue, Pgp(x) and I) Oatb2b1 normalized pmol/mg tissue, Oatp2b1(x). Experimental data when collected in-house are depicted by filled circles.

Figure 3. Feeding times and input functions. A) Experimental design for fasting and feeding schedule in rats. B) Schematic for design of input functions. Of the total dose, 10% was input as an immediate pulse, and the remaining 90% was input as a fast + slow pulse: fast pulse under fasted conditions + slow pulse from addition of food to 22 hr. Green: Fasted-0.5hr FT with 18% fast +72% slow pulse; Brown: Fasted-1hr FT with 36% fast +54% slow pulse, and Red: Fasted-2hr FT with 72% fast +18% slow pulse. C) Input function used for the Fasted-2hr FT group is depicted as an example. Note the broken X- and Y-axes depicted as such for visual clarity.

Figure 4. Individual and naïve-pooled average profiles for AML A) IV data (grey: individual and black: naïve-pooled average) and 2C-fitted lines. B) PO data for Fasted-2hr FT, C) PO data

for Fasted-1hr FT, and D) PO data for Fed group. Data displayed in blue indicate individual rat profiles. The black dots and line indicate the naïve-pooled average of the individual rat datasets.

Figure 5. Individual and naïve-pooled average profiles for DIG A) IV data (grey: individual and black: naïve-pooled average) and 2C-fitted lines. B) PO data for Fasted-1hr FT, C) PO data for Fasted-0.5hr FT, and D) PO data for Fed group. Data displayed in blue indicate individual rat profiles. The black dots and line indicate the naïve-pooled average of the individual rat datasets.

Figure 6. Individual and naïve-pooled average profiles for GLY A) IV data (grey: individual and black: naïve-pooled average) and 2C-fitted lines. B) PO data for Fasted-2hr FT, C) PO data for Fasted-1hr FT, and D) PO data for Fed group. Data displayed in blue indicate individual rat profiles. The black dots and line indicate the naïve-pooled average of the individual rat datasets.

Figure 7. Predicted C−t profiles with oral solution dose under different feeding conditions. Observed naïve-pooled average (blue points and line) and model-predicted (red) C−t profiles are overlaid upon normalization of AUC as described under Methods and Results. The green shaded region represents the overlapping area from time zero to last observed data collection time. Results are shown for (A) AML Fasted- 2 hr FT, (B) AML Fasted- 1 hr FT, (C) AML Fed, (D) DIG Fasted- 1 hr FT, (E) DIG Fasted- 0.5 hr FT, (F) DIG Fed, (G) GLY Fasted- 2 hr FT, (H) GLY Fasted- 1 hr FT, and (I) GLY Fed.

Tables

Table 1: Physicochemical properties, microsomal physicochemical partitioning, and Caco-2 permeability data for drugs

Compound (ionizability)	**Acid pK_a**	**Base pK_a**	**f_{um}[1]**	**Caco-2 P_{app} (x 10^{-6} cm/sec)[2]**
Amlodipine (base)	14	9.1	0.5	22.3
Digoxin (neutral)	7.15	1	0.63	4.42
Glyburide (acid)	5.1	1	0.72	18.9

[1] The f_{um} value for AML was predicted from our previously published model (Nagar and Korzekwa, 2017), GLY was measured in-house (Holt et al., 2019), and DIG was measured at Absorption Systems LLC.

[2]Sources for Caco-2 P_{app} values are as follows: AML from (Stader et al., 2020), DIG from (Djuv and Nilsen, 2008), and GLY from (Varma et al., 2014).

DMD Fast Forward. Published on March 26, 2022 as DOI: 10.1124/dmd.122.000831
This article has not been copyedited and formatted. The final version may differ from this version.

Table 2: Macro and micro compartmental PK parameter estimates and metrics of AML, DIG, and GLY calculated with a 2-compartmental model for naïve pooled average rat (n=3) upon an IV bolus dose. The naïve pool average estimates are listed as estimate ± standard error.

Parameter	**AML (2mg/kg)**	**DIG (0.25 mg/kg)**	**GLY (4 mg/kg)**
A (ng/mL)	271 ± 17.5	155 ± 5.37	13201 ± 367
α (hr^{-1})	5.55 ± 0.5	3.06 ± 0.21	3.75 ± 0.18
B (ng/mL)	86 ± 3.84	32.2 ± 3.63	2698 ± 162
β (hr^{-1})	0.24 ± 0.01	0.42 ± 0.03	0.390 ± 0.016
k12 (hr^{-1})	2.57 ± 0.13	1.10 ± 0.12	1.65 ± 0.1
k21 (hr^{-1})	1.26 ± 0.05	0.830 ± 0.035	0.96 ± 0.06
k10 (hr^{-1})	0.808 ± 0.03	1.45 ± 0.08	1.52 ± 0.04
Vc (mL)	1767 ± 45.5	441 ± 14.9	73.9 ± 1.76
CL (mL/hr)	1442 ± 80	1924 ±167	112.4 ± 6.0
VDss (mL)	5321 ± 590	3032 ±527	201.2 ± 21
$t_{1/2}$ (hr)	2.89 ± 0.23	1.66 ±0.20	1.78 ± 0.13
$AUC_{(0-\infty)}$ (ng•hr/mL)	407.2 ± 23	127.7 ±11	10448 ± 539

DMD Fast Forward. Published on March 26, 2022 as DOI: 10.1124/dmd.122.000831
This article has not been copyedited and formatted. The final version may differ from this version.

Table 3: Observed and predicted Cmax, tmax, and exposure overlap coefficients (EOC) for AML, DIG, and GLY. Observed metrics are listed based on the naïve-pooled datasets.

Drug	Group	$AUC_{0\text{-}inf}$ obs (ng.h/ml)	Cmax obs (ng/ml)	Cmax pred (ng/ml)	tmax obs (h)	tmax pred (h)	EOC
AML	Fasted- 2 hr FT	274	34.8	39.4	2.5	2.5	0.92
	Fasted- 1 hr FT	435	36.6	51.3	4.0	1.2	0.89
	Fed	475	18.6	18.2	21.8	19.6	0.97
DIG	Fasted- 1 hr FT	77	11.1	11.1	0.7	1.5	0.88
	Fasted- 0.5 hr FT	80	10.1	7.84	0.2	1.3	0.80
	Fed	193	13.5	8.0	0.2	1.9	0.84
GLY	Fasted- 2 hr FT	5.1	2.18	1.20	1.5	2.3	0.82
	Fasted- 1 hr FT	4.8	0.50	0.5	0.5	1.4	0.93
	Fed	3.6	0.19	0.15	2.5	9.7	0.94

DMD Fast Forward. Published on March 26, 2022 as DOI: 10.1124/dmd.122.000831
This article has not been copyedited and formatted. The final version may differ from this version.

Figure 1

A.

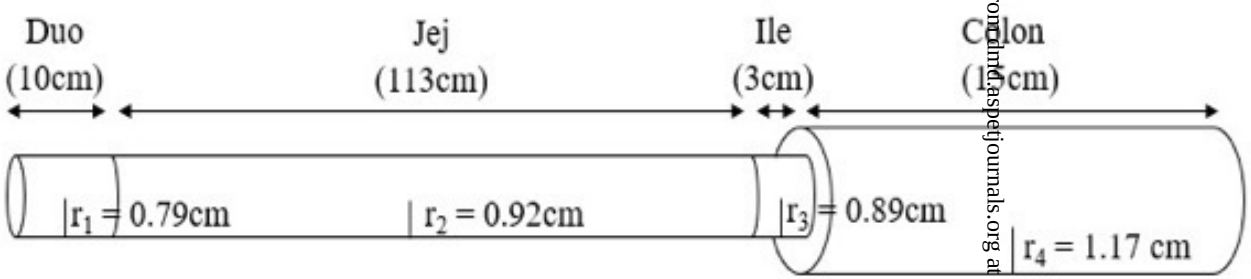

B.

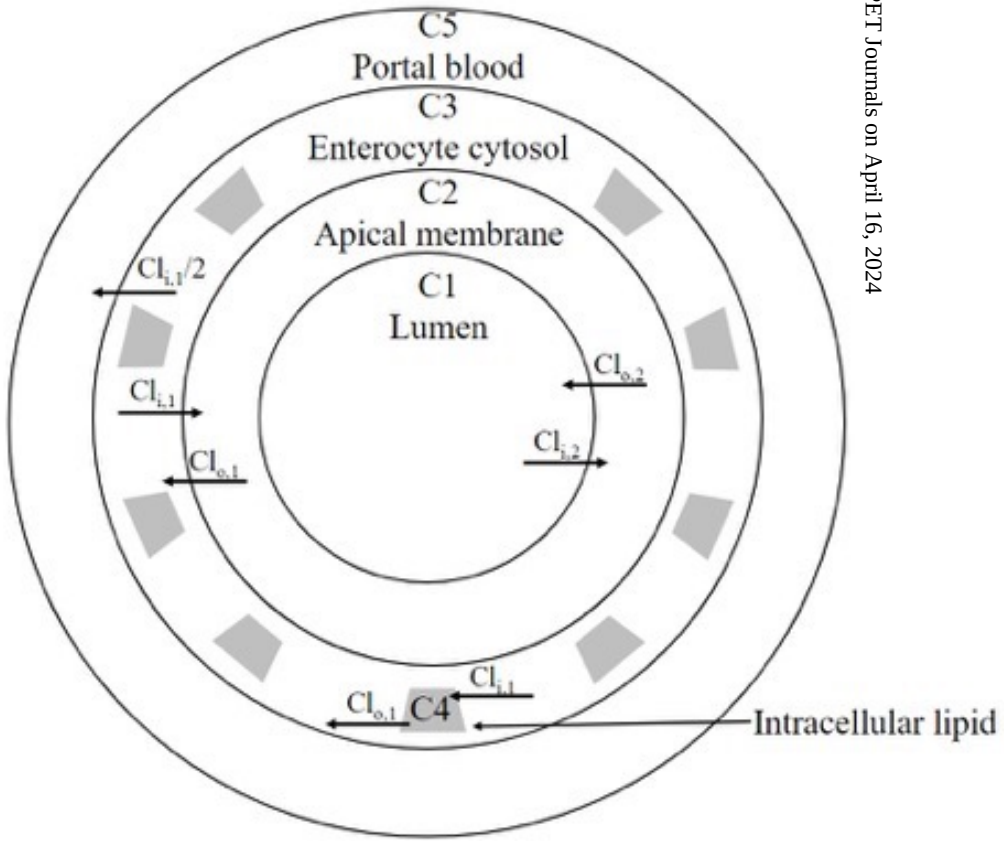

Figure 2.

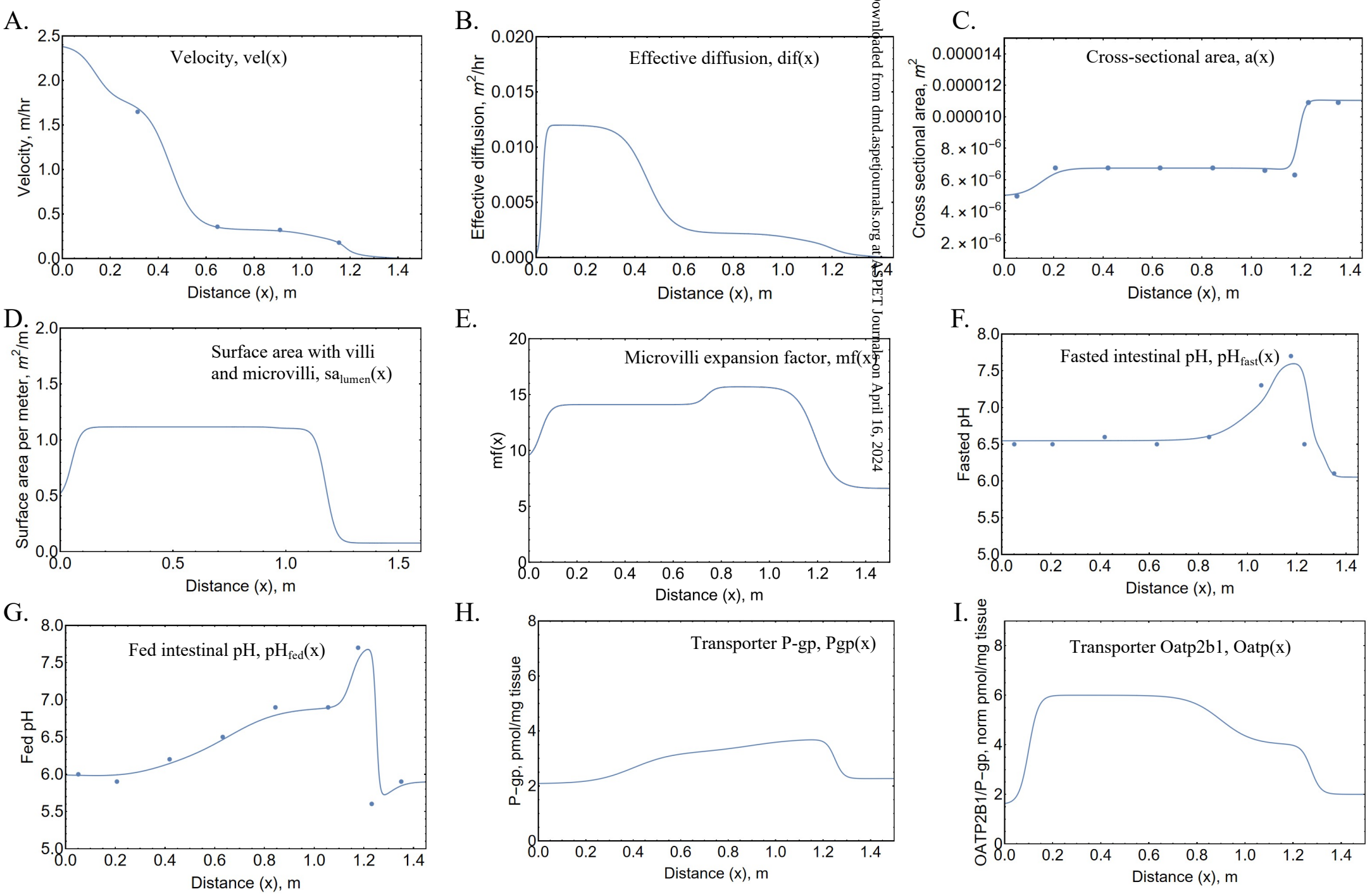

Figure 3.

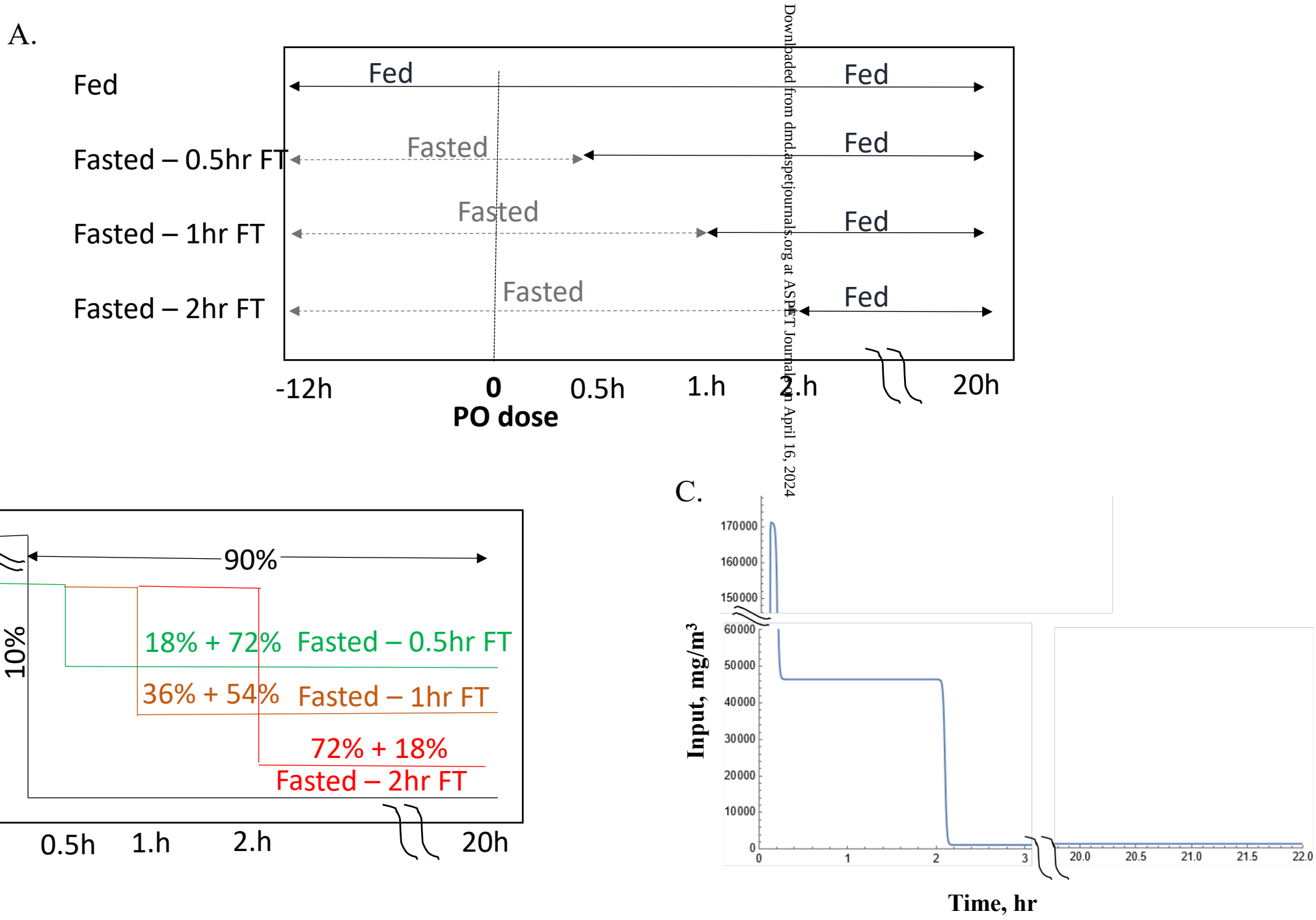

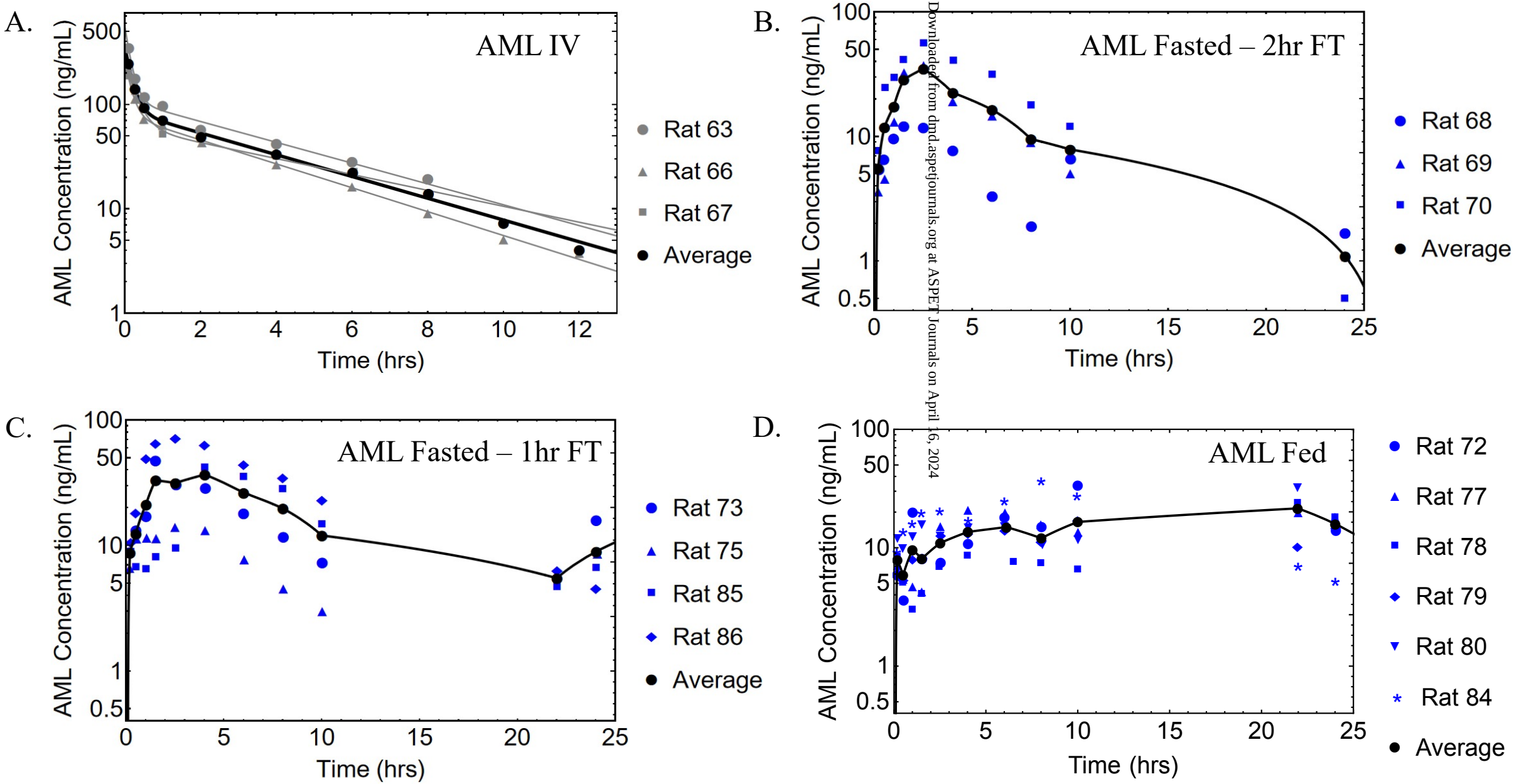

Figure 4

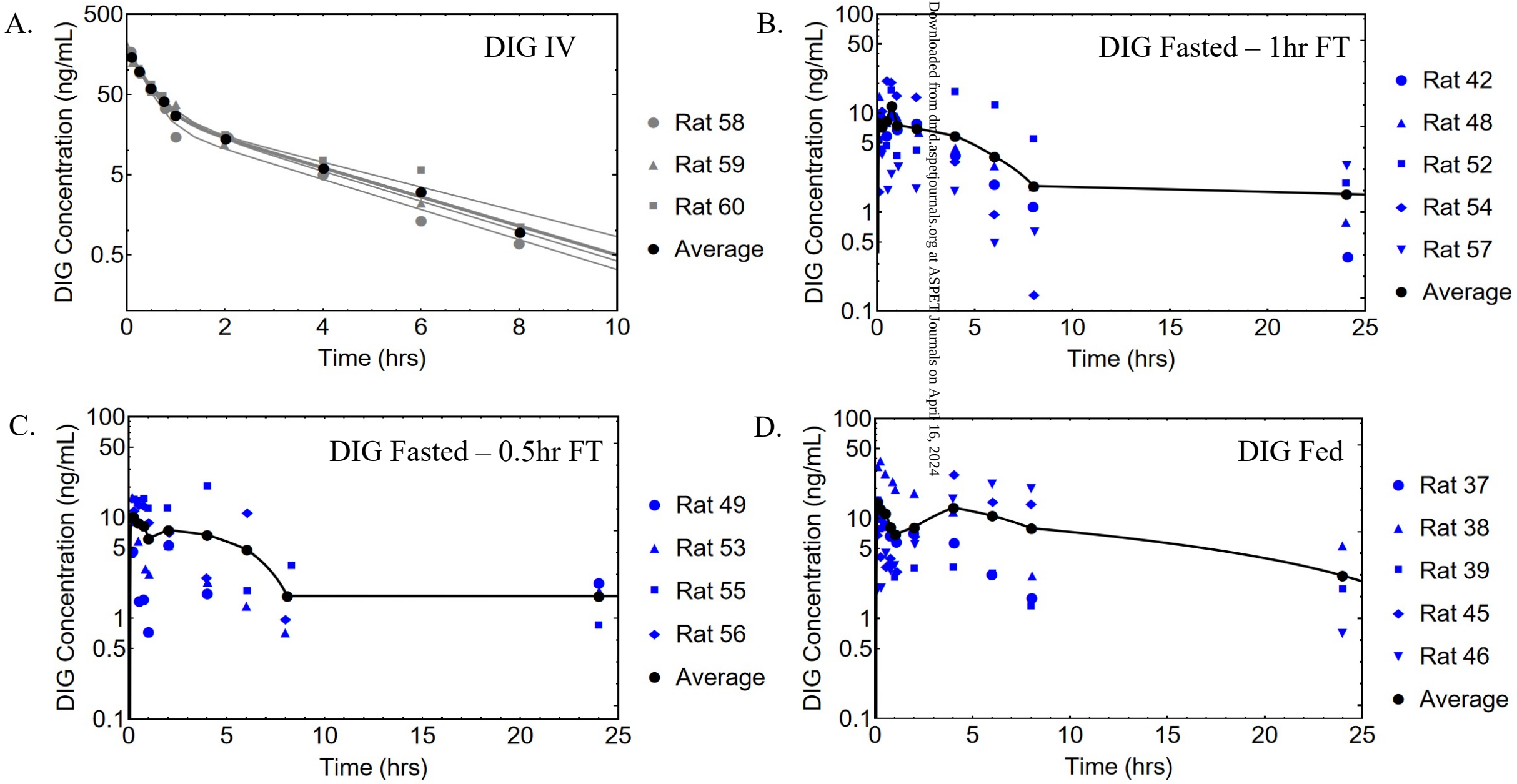

Figure 5

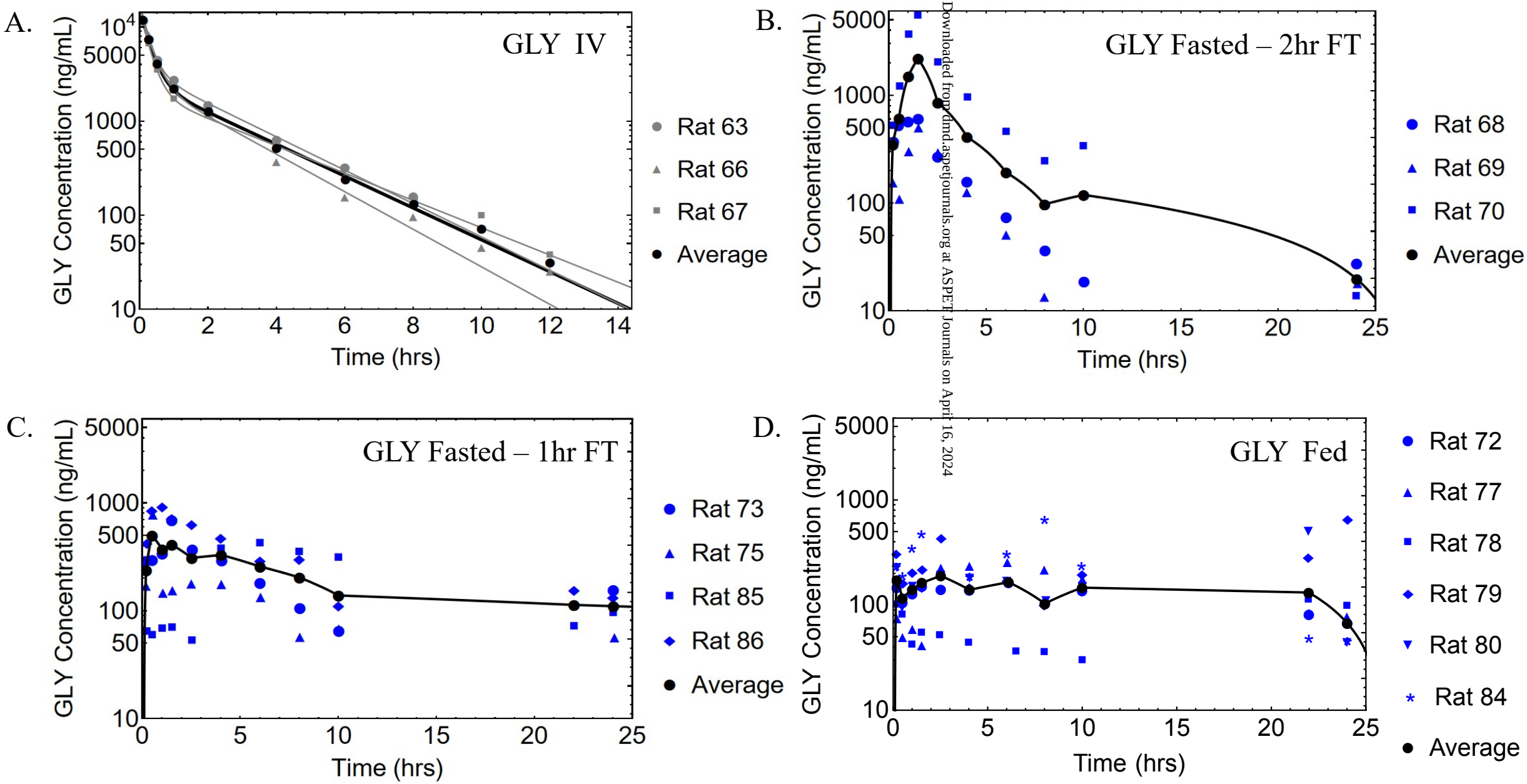

Figure 6

Figure 7